Viscous Flow over Spinning Cones at Angle of Attack

T. C. LIN*
NASA-Marshall Space Flight Center, Huntsville, Ala.
AND
S. G. RUBIN†
Polytechnic Institute of New York, Farmingdale, N.Y.

A numerical finite-difference method is developed for evaluating the Magnus coefficients on spinning cones in laminar flow. The merged layer, the strong interaction region, the downstream boundary layer and boundary region are all considered. The numerical method is an iterative predictor-corrector scheme developed for three-dimensional flow with or without crossflow diffusion. This method is particularly useful for problems in which a symmetry plane does not exist. Several contributions to the Magnus force and moments are considered. These include asymmetries in displacement thickness, centrifugal force and crossflow shear, and the effects of crossflow separation and vortex formation. Comparisons are made with experimental data and other theoretical analyses.

Nomenclature

C_m	= pitching moment (Eq. (12)
C_y	= Magnus force coefficient (Eq. 10)
L	= characteristic length
M_∞	= freestream Mach number
Pr	= Prandtl number
p	= pressure
$Q = \frac{1}{2}\rho_\infty u_\infty^2$	= dynamic pressure
$Re = \rho_\infty u_\infty L/\mu_\infty$	= Reynolds number
r	= radius
S	= cone base area
T	= temperature
u, v, w	= velocities along x, y, ϕ coordinates
$V_\infty = M_\infty[c/(Re \cdot x)]^{1/2}$	= rarefaction parameter
x, y, ϕ	= coordinates (see Fig. 1)
α	= angle of attack
γ	= ratio of specific heats
δ	= displacement thickness
θ	= cone half angle
ξ, l, z	= coordinates (see Fig. 1)
ρ	= density
Ω	= $r\omega/u_\infty$
ω	= angular velocity of spinning in revolutions per minute

Subscripts

e	= conditions refer to boundary-layer edge
t	= stagnation condition
w	= conditions refer to cone surface
∞	= conditions refer to freestream

I. Introduction

MAGNUS phenomena have been investigated, both experimentally and theoretically, by a number of authors. Useful summaries are provided by Platou[1] and Fletcher.[2] Generally speaking, the force and moment induced by spin are small. However, the Magnus effect cannot be neglected on spin-stabilized shells or rockets, as it may tend to undamp the projectile.

Most of the theoretical analyses concerned with compressible viscous flow on rotating cones have been limited to the case of small incidence without separation. Illingworth[3] analyzed the flow around a spinning cone at zero incidence. Sedney[4] was the first to consider the effects of angle of attack. He developed a perturbation procedure based on Martin's[5] postulate that the Magnus force is primarily induced by the asymmetric effective body shape associated with viscous displacement. Clark[6] has recently obtained Navier-Stokes solutions for spinning ellipsoids but only for low Reynolds number and incompressible flow. Dwyer[7] considered the three-dimensional boundary layer on a cone by a finite-difference method; however, he was unable to obtain unique solutions at the leeward plane. As noted by Dwyer, his numerical formulation results in an improperly posed initial value problem. Furthermore, in order to start his calculation, flow profiles at the windward plane must be prescribed at each streamwise station. These are initially unknown and therefore can only be approximated. Watkins[8] solved the initialization problem by constructing flow profiles at the windward plane from a perturbation analysis for small spin. He duplicated Dwyer's procedure for an ogive cylinder where leeward plane difficulty was not encountered. This is apparently due to the different streamwise and azimuthal pressure gradients found on cones and ogive cylinders. The Magnus coefficients were not discussed.

Recently Vaughn and Reis[9] developed an analytical approximate solution for spinning projectiles. Their formulation includes the effects of viscous displacement and centrifugal force, and their theory applies to both supersonic and subsonic flows. These solutions were obtained from relatively simple analytic formulas and should be particularly useful for engineering design purposes. However, their flow profiles are approximate, and the authors did not include the crossflow drag force which, as will be shown later, can become significant.

In this paper, we intend to develop a numerical model to describe the Magnus phenomenon. The differences between this approach and those previously discussed are: 1) the contributions to the Magnus coefficients include the asymmetric viscous displacement effect, centrifugal force, cross-stream skin friction, and the influence of secondary flow reversal; 2) the lateral diffusion terms are retained and are essential if accurate and unique solutions are to be obtained‡; 3) windward plane solutions are not required to initiate cross-plane calculations; 4) an efficient predictor-corrector numerical scheme is applied,

Presented at the AIAA Computational Fluid Dynamics Conference, Palm Springs, Calif., July 19–20, 1973; submitted September 13, 1973; revision received January 24, 1974. This research was supported in part by the Air Force Office of Scientific Research under Grant AFOSR 70-1843 and Modification AFOSR 70-1843A, Project 9781-01. The U.S. Government is authorized to reproduce and distribute reprints for Governmental purposes, notwithstanding any copyright notation hereon.

Index categories: Boundary Layers and Convective Heat Transfer—Laminar; Rarefied Flows; Viscous Nonboundary-Layer Flows.

* NRC-NASA Postdoctoral Research Associate in Aero-Astrodynamics Laboratory; currently Staff Scientist, Avco System Division, Wilmington, Mass.

† Professor. Associate Fellow AIAA.

‡ Independently, Dwyer[7] has also suggested to include the lateral diffusion terms in order to obtain unique solutions at leeward plane.

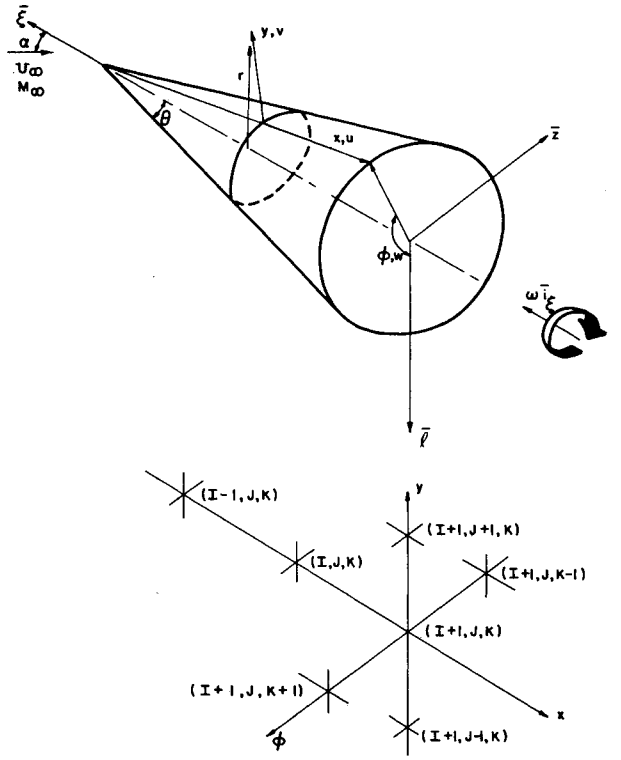

Fig. 1 Coordinate system.

which can handle problems with or without crossflow separation and does not require any symmetric boundary conditions; and 5) unique solutions for a cone are obtained at the leeward generator. The latter result is a direct consequence of condition (2).

From recent experimental data as well as various theoretical investigations, the different flow regions on a slender body moving at supersonic speed have been defined and differentiated. At the leading edge, a small free-molecular regime occurs while far downstream, in the weak interaction region, a distinct outer inviscid flow and inner boundary layer appear. Joining these two limiting domains are the so-called "merged layer" and "strong interaction" regions, where the outer shock wave is initially not of Rankine-Hugoniot type, and surface slip effects may be important. The boundary-layer and "shock" behavior are coupled throughout these regions. In this paper Magnus effects on the flow behavior from the merged layer through the weak interaction region are discussed. Solutions for the tip merged layer and strong interaction region are given in Sec. II. The formulation for the supersonic boundary region that forms downstream of the tip is discussed in Sec. III. In Sec. IV a predictor-corrector numerical scheme previously developed by the authors is reviewed. Finally, the results and evaluation of the Magnus coefficients are presented in Sec. V.

II. Merged Layer

At high speed and/or low Reynolds numbers, a rather large merged layer region occurs near the tip of a cone. In this region viscous effects are dominant and shock-boundary layer merging occurs. A detailed discussion of these flows for nonrotating cones at zero incidence is given by Rubin et al.,[15] Novack and Cheng,[16] and Rubin and Lin.[17] A brief review will now be presented. A single-layer model is prescribed wherein the entire disturbed flow including shock waves, boundary layers, and inviscid core regions are calculated without the necessity of matching. The governing equations are a parabolized version of the Navier-Stokes equations including crossflow diffusion and streamwise pressure gradients. This system represents a uniformly valid first approximation for the complete disturbed flow. Except for the surface conditions on the crossflow velocity w, the boundary and initial conditions are identical with those for the zero spin flow.[10] The reduced merged layer equations for flow at incidence are as follows (see Fig. 1 for notations).

Continuity

$$(\rho u)_x+(\rho v)_y+\frac{1}{r}[\rho u\Gamma+\rho v\cos\theta+(\rho w)_\phi]=0 \tag{1a}$$

x-Momentum

$$\rho uu_x+\rho vu_y+\frac{\rho w}{r}u_\phi-\frac{\rho w^2}{r}\Gamma\frac{1}{M_\infty{}^2\gamma}+\frac{1}{M_\infty{}^2\gamma}p_x=\frac{1}{r}(\mu ru_y)_y+\frac{1}{r^2}(\mu u_\phi)_\phi-\frac{1}{M_\infty{}^2\gamma}\frac{\mu}{r^2}\Gamma w_\phi \tag{1b}$$

$$\rho uv_x+\rho vv_y+\frac{\rho w}{r}v_\phi-\frac{\rho w^2}{r}\cos\theta+p_y=\tfrac{4}{3}(\mu v_y)_y+\frac{1}{r^2}(\mu v_\phi)_\phi+\mu_x u_y+\tfrac{1}{3}\mu u_{xy}-\tfrac{2}{3}\mu_y u_x-\tfrac{2}{3}\mu_y\frac{1}{r}[u\Gamma+v\cos\theta+w_\phi]+\frac{\mu_\phi}{r}w_y-\frac{\mu_\phi}{r^2}w\cos\theta+\frac{\mu}{3r}u_y\Gamma+\frac{4\mu}{3r}\cos\theta\left(v_y-\frac{v\cos\theta+u\Gamma}{r}\right)+\frac{\mu}{3r}w_{y\phi}-\frac{7}{3}\frac{\mu}{r^2}\cos w_\phi \tag{1c}$$

and

$$\rho uw_x+\rho vw_y+\frac{\rho w}{r}w_\phi+\frac{\rho uw}{r}\Gamma+\frac{\rho vw}{r}\cos\theta+\frac{1}{r}p_\phi=(\mu w_y)_y+\frac{\mu}{r}\cos\theta w_y+\frac{4}{3r^2}(\mu w_\phi)_\phi+\frac{7}{3}\frac{\mu v_\phi}{r^2}\cos\theta+\frac{\mu}{3r}v_{y\phi}+\mu_\phi\left[\frac{4}{3r^2}(v\cos\theta+u\Gamma)-\frac{2}{3r}(u_x+v_y)\right]+\frac{1}{3r}\mu u_{x\phi}+\mu_y\left[\frac{v_\phi}{r}-\frac{w}{r}\cos\theta\right]+\frac{4}{3}\frac{\Gamma}{r^2}\mu u_\phi-\frac{\mu}{r^2}w\cos^2\theta+u_\phi\left[\frac{\mu\Gamma}{r^2}+\frac{\mu x}{r}\right]-\frac{\mu w}{r^2}\frac{1}{M_\infty{}^2\gamma}\Gamma^2+\frac{\mu\Gamma w_x}{r}\frac{1}{M_\infty{}^2\gamma} \tag{1d}$$

Energy

$$\rho uT_x+\rho vT_y+\frac{\rho w}{r}T_\phi+p(\gamma-1)\left[u_x+v_y+\frac{u\Gamma+v\cos\theta+w_\phi}{r}\right]=\frac{\gamma}{\sigma}(\mu T_y)_y+\frac{\gamma}{\sigma}\frac{\mu}{r}\cos\theta T_y+\frac{\gamma}{\sigma}\frac{1}{r^2}(\mu T_\phi)_\phi+\frac{\mu(\gamma-1)}{r^2}w^2\sin^2\theta+\tfrac{4}{3}\mu(\gamma-1)\left\{v_y{}^2+\frac{1}{r^2}(u\Gamma+v\cos\theta+w_\phi)^2\right\}-\frac{2\mu}{r^2}M_\infty{}^2\gamma(\gamma-1)u_\phi w\sin\theta\delta+\mu(\gamma-1)\times\left[w_y+v_\phi\frac{1}{r}-\frac{w\cos\theta}{r}\right]^2+M_\infty{}^2\gamma(\gamma-1)\mu\left[u_y{}^2+\frac{1}{r^2}u_\phi{}^2\right]-\tfrac{4}{3}\mu(\gamma-1)v_y\left(\frac{w_\phi+u\Gamma+v\cos\theta}{r}\right) \tag{1e}$$

State

$$p=\rho T$$

where the dimensional coordinates $\bar{x}$, $\bar{y}$ are nondimensionalized with $\bar{\mathscr{L}}$, $\bar{\mathscr{L}}\delta$, respectively, and velocities $\bar{u}$, $\bar{v}$, and $\bar{w}$ with $\bar{U}_\infty$, $\delta\bar{U}_\infty$ and $\bar{U}_\infty\delta$; and

$$\bar{\mathscr{L}}=M_\infty{}^3\gamma\bar{\mu}_\infty/\bar{\rho}_\infty\bar{U}_\infty;\quad \delta=[(\gamma)^{1/2}M_\infty]^{-1};\quad \Gamma=\theta/\delta$$

θ = half angle of cone: $\Delta^2=T_{\text{ref}}/\gamma M_\infty{}^2$; $T=\bar{T}/\bar{T}_\infty$

$p=\bar{p}/\bar{p}_\infty$; $\mu=\bar{\mu}/\bar{\mu}_\infty\bar{M}_\infty$; $r=\bar{r}/\delta\bar{\mathscr{L}}=x\Gamma+y\cos\theta$

σ = Prandtl number; $\gamma=c_p/c_v$;

M_∞ = freestream Mach Number

$$Re=\bar{\rho}_\infty\bar{u}_\infty/\bar{\mu}_\infty;\quad \bar{v}=M_\infty(c/Re\,\bar{x})^{1/2};\quad \bar{\chi}=M_\infty{}^3(c/Re\,\bar{x})^{1/2}$$

These equations are independent of the unit Reynolds number, Re, and represent a uniformly valid first approximation for the entire flow, with an error corresponding to the largest of Δ^2, δ^2, or θ^3/δ. The governing system is of parabolic or hyperbolic form when the P_x term in the x-momentum equation is treated explicitly or when a constant pressure subsonic sublayer is prescribed. A detailed treatment of P_x is given in Ref. 11. A streamwise marching technique is used to solve the resulting initial value problem. Slip boundary conditions are prescribed at the wall

$$y=0, \quad u=\lambda_1 u_y, \quad T=T_w+\lambda_2 T_y$$

$$w=\lambda_1\left[w_y+\frac{3}{(8\pi T)^{1/2}}\frac{T_\phi}{r}\right]+\frac{r\omega}{u_\infty}\frac{M_\infty{}^3\gamma}{Re}$$

$$\lambda_1=1.26\mu/\rho T^{1/2}, \quad \lambda_2=\frac{2\gamma}{(\gamma+1)}\frac{\lambda_1}{Pr}$$

$$T_w=\bar{T}_w/\bar{T}_\infty$$

Symmetry conditions are not invoked at the windward or leeward planes. Instead, continuity of the flow profiles at $\phi=0$ and 2π is imposed.

Freestream properties apply as $y\to\infty$; i.e.,

$$u=\cos\alpha\cos\theta-\sin\alpha\cos\phi\sin\theta$$

$$v=-[\cos\alpha\sin\theta+\sin\alpha\cos\phi\cos\theta]/\delta$$

$$w=\sin\alpha\sin\phi/\delta$$

$$T=p=\rho=1; \quad \text{and} \quad \delta=[(\gamma)^{1/2}M_\infty]^{-1}$$

III. Boundary Region Formulation

Downstream of the cone tip where merging and strong interactions are no longer important, supersonic boundary-layer theory can be applied. Here the conventional boundary-layer equations are modified to include all pertinent effects of crossflow diffusion and centrifugal force. With the usual boundary-layer approximations $\partial/\partial y \gg \partial/\partial x$, $Re\gg 1$ and the retention of cross-diffusion terms, required to adequately describe boundary regions or local shear flows formed near separation planes, so that $(1/r)(\partial/\partial\phi)=0(\partial/\partial y)$ locally, the Navier-Stokes equations reduce to

Continuity

$$x(\rho u)_x-\frac{\eta}{2}(\rho u)_\eta+(\rho v)_\eta+\frac{x}{r}\left[\sin\alpha(\rho w)_\phi+\rho u\sin\theta+\rho v(Re\cdot x)^{-1/2}\cos\theta\right]=0 \tag{2a}$$

x-Momentum

$$x\rho u u_x-\frac{\eta}{2}\rho u u_\eta+\rho v u_\eta+\frac{\rho w\sin\alpha}{r}xu_\phi-\frac{x}{r}\rho w^2\sin^2\alpha\sin\theta=-\frac{x}{M_\infty{}^2\gamma}p_x+(\mu u_\eta)_\eta+\left(\frac{x}{Re}\right)^{1/2}\frac{\mu}{r}\cos\theta u_\eta+\frac{x}{r^2}\frac{1}{Re}[(\mu u_\phi)_\phi] \tag{2b}$$

y-Momentum

$$p_\eta=M_\infty{}^2\gamma\sin^2\alpha x^{1/2}Re^{-1/2}\frac{\rho w^2\cos\theta}{r} \tag{2c}$$

ϕ-Momentum

$$x\rho w_x u-\frac{\eta}{2}\rho u w_\eta+\rho v w_\eta+\frac{\rho w\sin\alpha}{r}xw_\phi+\frac{\rho uw}{r}x\sin\theta=-\frac{x}{rM_\infty{}^2\gamma\sin\alpha}p_\phi+(\mu w_\eta)_\eta+\left(\frac{x}{Re}\right)^{1/2}\frac{\mu}{r}\cos\theta w_\eta+\frac{4}{3}\frac{x}{Re\,r^2}(\mu w_\phi)_\phi \tag{2d}$$

Energy

$$x\rho u T_x-\frac{\eta}{2}\rho u T_\eta+\rho v T_\eta+\frac{\rho w\sin\alpha}{r}xT_\phi+p(\gamma-1)x\left[u_x-\frac{1}{2}\frac{\eta}{x}u_\eta+\frac{u\sin\theta}{r}+\frac{\sin\alpha}{r}w_\phi+\frac{v_\eta}{x}+\frac{v}{r}\cos\theta(Re\cdot x)^{-1/2}\right]=\frac{\gamma}{Pr}\left[(\mu T_\eta)_\eta+\left(\frac{x}{Re}\right)^{1/2}\frac{\mu}{r}\cos\theta T_\eta\right]+M_\infty{}^2\gamma(\gamma-1)\mu[u_\eta{}^2+\sin^2\alpha w_\eta{}^2]+\frac{1}{r^2}\frac{x}{Re}\left[\mu M_\infty{}^2\gamma(\gamma-1)(u_\phi{}^2+\tfrac{4}{3}\sin^2\phi w_\phi{}^2+\sin^2\alpha\cos\theta w^2)+\frac{\gamma}{Pr}(\mu T_\phi)_\phi\right] \tag{2e}$$

State

$$p=\rho T \tag{2f}$$

where

$$r=x\sin\theta+\eta\cos\theta\left(\frac{x}{Re}\right)^{1/2}, \quad Re=\bar{\rho}_\infty\bar{u}_\infty L/\bar{\mu}_\infty,$$

$$\eta=\bar{y}\left(\frac{Re}{x}\right)^{1/2}\Big/L,$$

$$x=\bar{x}/L, \quad \mu=\bar{\mu}/\bar{\mu}_\infty, \quad u=\bar{u}/\bar{u}_\infty, \quad v=\bar{v}[Re\cdot x]^{1/2}/u_\infty,$$

$$w=\bar{w}/\bar{u}_\infty\sin\alpha, \quad \rho=\bar{\rho}/\bar{\rho}_\infty, \quad L=1'' \text{ or } 1',$$

$\alpha=$ angle of attack, and $\theta=$ cone half angle.

The coordinate system as depicted in Fig. 1 is attached to the cone surface and does not rotate with the body. The governing system is not restricted to small crossflow. The retention of azimuthal diffusion terms has been found to be important in regions where crossflow separation occurs and when the boundary layer exhibits a local nonsimilarity. Without these terms, the numerical integration encounters instability in these regions. Significantly, the secondary flow separation line is not a singular point in this formulation.

The boundary conditions for the boundary layer flow are

$$\eta=0, \quad u=v=0, \quad w=r\omega/u_\infty\sin\alpha, \quad T=T_w \text{ or } T_\eta=0; \quad \eta=\infty, \quad u=u_e, \quad w=w_e, \quad T=T_e \tag{2g}$$

Once again the windward and leeward surfaces are not symmetry planes for the spinning cone; rather, a periodic continuation of the flow profiles at $\phi=0$ and 2π is specified.

Initial conditions are specified at $x=0.05$, where the zero spin results of Lin and Rubin[10,12] are postulated. The outer inviscid data are assumed to be conical and unaffected by the rotation. This approximation is reasonable in view of the merged layer results for the surface pressure distribution. This simplification is correct to zeroth order as seen from Kelly[19] and Martin's[5] theory for which the Magnus force is $O[1/(Re\cdot x)^{1/2}]$ in laminar flow. Jones'[20] tabulated results can be employed to obtain external conditions. The vorticity and viscous displacement interactions have been assumed to be higher order and hence negligible in the present analysis. Recently Mayne[21] has considered the effects of "streamline or entropy swallowing." His boundary layer results indicate that these effects are small for the geometry and Mach numbers considered here.

IV. Numerical Finite-Difference Scheme

The numerical scheme considered here is a predictor-corrector (P/C) iterative technique. This method, developed by the present authors, has been applied satisfactorily for a variety of three-dimensional merged[10,11] and boundary-layer problems.[12] With an implicit backward difference formulation, the following difference quotients are postulated (see Fig. 1 for notation):

$$u_x=\frac{1}{2\Delta x}[3u_{I+1,J,K}^{(m+1)}-4u_{I,J,K}+u_{I-1,J,K}]$$

$$u_y=\frac{1}{2\Delta y}[u_{I+1,J+1,K}^{(m+1)}-u_{I+1,J-1,K}^{(m+1)}]$$

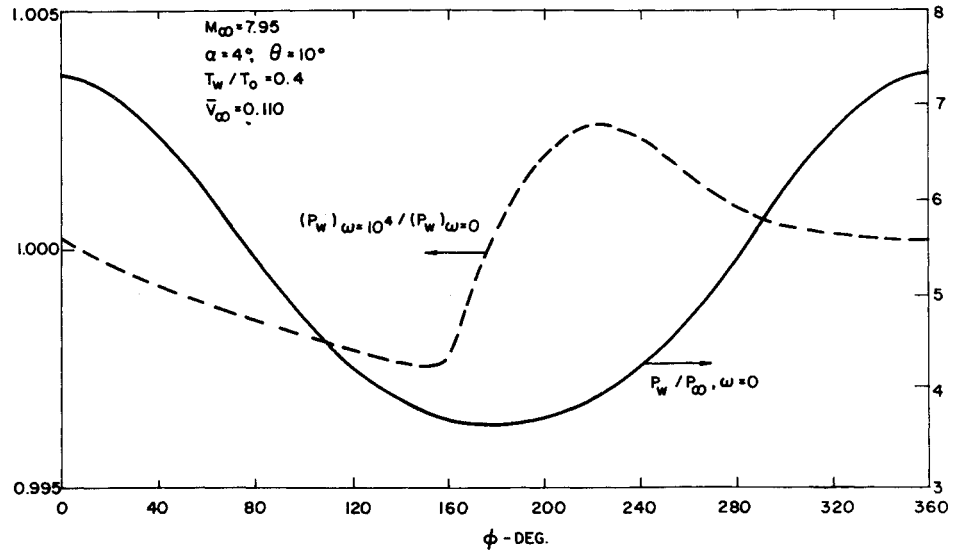

Fig. 2 Surface pressure distribution-merged layer.

$$u_{yy} = \frac{1}{\Delta y^2}\left[u_{I+1,J+1,K}^{(m+1)} + u_{I+1,J-1,K}^{(m+1)} - 2u_{I+1,J,K}^{(m+1)}\right]$$

$$u_{\phi} = \frac{1}{2\Delta\phi}\left[u_{I+1,J,K+1}^{(m)} - u_{I+1,J,K-1}^{(L)}\right]$$

$$u_{\phi\phi} = \frac{1}{\Delta\phi^2}\left[u_{I+1,J,K+1}^{(m)} + u_{I+1,J,K-1}^{(L)} - 2u_{I+1,J,K}^{(m+1)}\right].$$

The superscripts m and L denote the iteration number with all I, $I-1$ subscript variables known. When the superscript $L = m$, Jacobi-type iteration results, and when $L = m+1$, Gauss-Seidal iteration results. In the latter case, the most recent iterates are used when they become available. The initial predictor value, superscript zero, is obtained from a Taylor series extrapolation:

$$u_{I+1,J,K}^{(0)} = 3u_{I,J,K} - 3u_{I-1,J,K} + u_{I-2,J,K} + 0(\Delta x^3).$$

As shown by Rubin and Lin,[11] the number of iterations necessary to achieve second-order accuracy of this P/C method is significantly decreased with third-order accurate initial predictor values. Nonlinear terms, such as $[u_{I+1,J,K}^{(m+1)}]^2$ are linearized by a first-order Newton-Raphson procedure. In general, if $f = f(P_1, P_2 \ldots P_k) = f(P_i)$, then

$$f^{(m+1)} = f^{(m)} + \sum_{i=1}^{k} \frac{\partial f}{\partial P_i}(P_i^{(m+1)} - P_i^{(m)}).$$

The P_i denotes the dependent variables. When $f = u_{I+1,J,K}^2$, then

$$[u_{I+1,J,K}^{(m+1)}]^2 = 2u_{I+1,J,K}^{(m+1)} u_{I+1,J,K}^{(m)} - [u_{I+1,J,K}^{(m)}]^2$$

The resulting finite-difference system is solved by an efficient algorithm.[10]

The predictor-corrector method described herein is implicit in the surface normal direction in which the steepest gradients appear. With proper use of iteration, lateral grid size induced instability is minimized, and the accuracy and consistency of the finite-difference solution is improved. For $m \geqq 1$, the stability restriction is

$$(r\Delta\phi/\Delta x) \geqq (w/u)$$

This condition is independent of the choice of the normal grid size Δy as well as the Reynolds number. An additional analysis relating to the P/C approach and concerning the effects of nonlinearity, iteration, and consistency is given by Rubin and Lin,[11] and Rubin.[13] Recently Helliwell and Lubard[14] have successfully employed a similar P/C method.

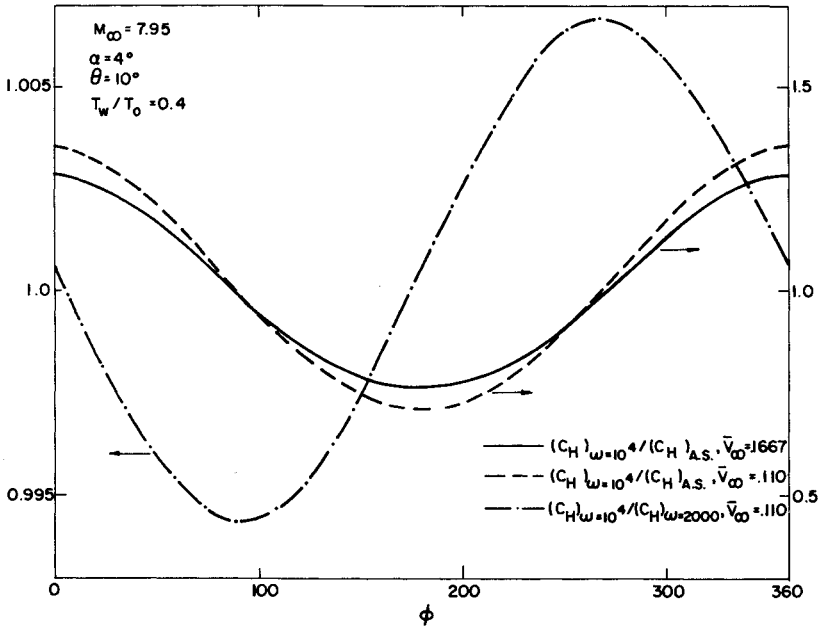

Fig. 3 Normalized heat-transfer distribution-merged layer.

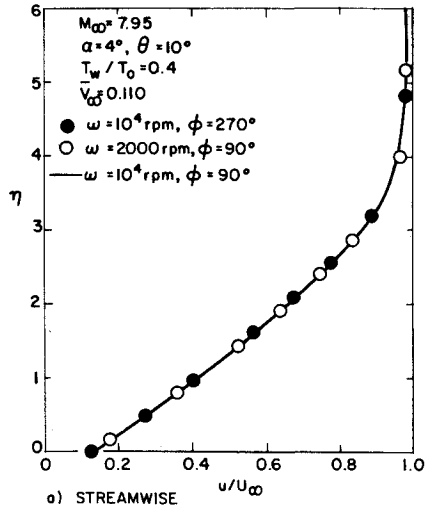

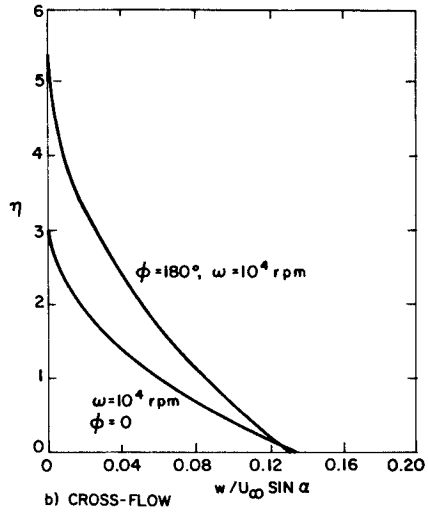

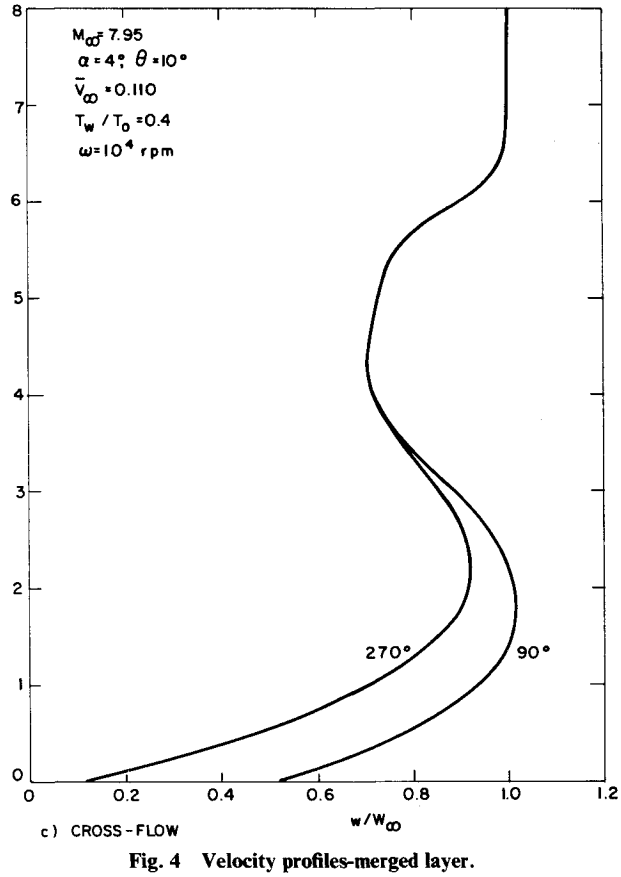

Fig. 4 Velocity profiles-merged layer.

V. Results and Magnus Coefficients

The Magnus force and moments are the result of asymmetries in 1) centrifugal force; 2) crossflow drag; 3) viscous displacement; 4) secondary flow separation and vortex formation; and 5) transition to turbulent flow. Only the first four contributions will be discussed here. It should be noted that the asymmetric transition from laminar to turbulent boundary layer can have a significant effect on the Magnus forces.[2,22]

A) Merged Layer Results

Most of the numerical computations for the merged layer region considered here correspond to the experimental conditions of Tracy.[18] Figure 2 depicts surface pressure distributions at spin values $\omega = 0$ and $\omega = 10^4$ rpm. The rotation effect is found to be minimal throughout this angular velocity range. The wall pressure is slightly larger on the advancing side than on the retreating side of the cone. The side force or Magnus effect that results from the asymmetric pressure distribution is therefore small. This should be expected since $\Omega = r\omega/u_\infty \ll 1$ near the tip of the cone. The heat-transfer distributions are given in Fig. 3. It can be seen that C_H decreases when the rotation is in the direction of the external flow (retreating side), whereas it increases when the two velocities oppose each other (advancing side). The streamwise velocity profile is almost identical (to three significant figures) in all cases (Fig. 4a), although a considerable difference is found between the crossflow profiles at $\phi = 90°$ and 270° (Fig. 4c). Therefore, spin, unlike injection or surface heating, has only a small influence on the flow surface properties in the merged region.

B) Boundary Region Results

The contribution due to the centrifugal force can be estimated from Eq. (2c). Integrating across the boundary layer, we obtain

$$p_w = p_e - \int_0^{\eta_\delta} M_\infty{}^2 \gamma \sin^2\alpha \left(\frac{x}{Re}\right)^{1/2} \frac{\rho w^2}{r} \cos\theta \, d\eta \qquad (3)$$

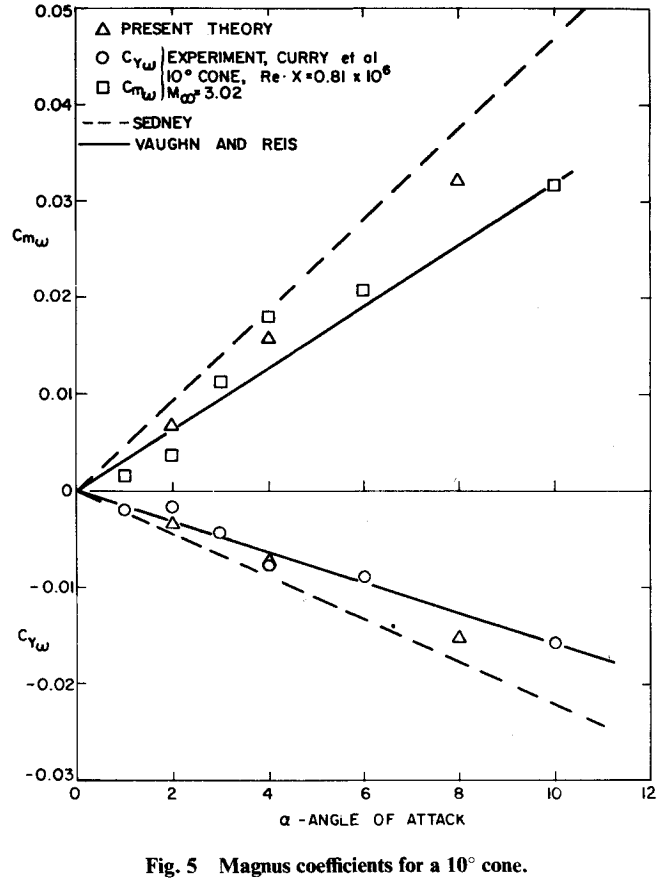

Fig. 5 Magnus coefficients for a 10° cone.

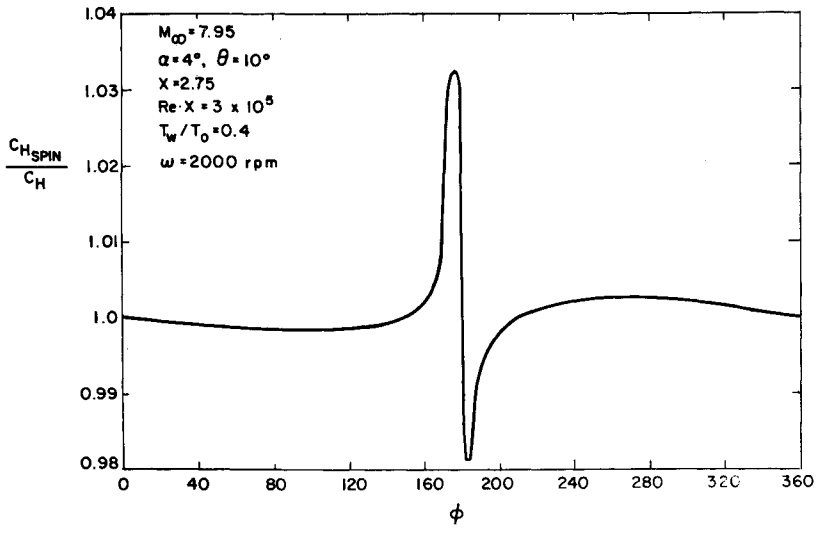

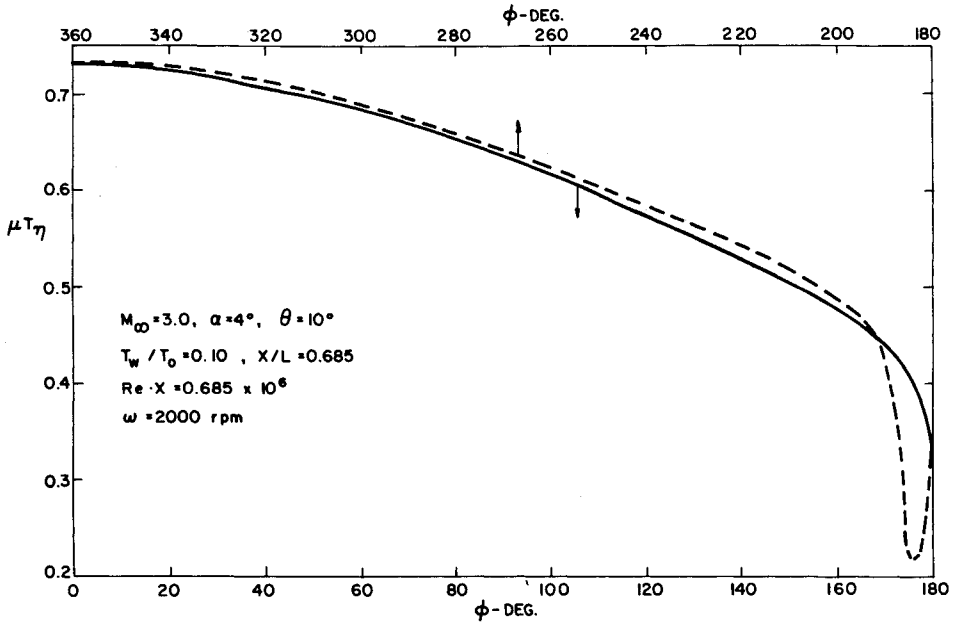

Fig. 6 Azimuthal distribution of heat transfer.

Since p_e is assumed to be unaffected by spin, the second term on the right-hand side will provide the only nonzero contribution. The integrated value becomes

$$(\bar{C}_f)_{cf} = \frac{\bar{f}_{cf}}{QS} = -\frac{2\sin^2\alpha\cos\theta}{S(Re)^{1/2}} \times$$

$$\bar{i}_z \int_0^x (x)^{1/2}\,dx \int_0^{2\pi} \sin\phi\,d\phi \int_0^\infty \left\{\frac{\rho w^2\,d\eta}{1+\{\eta/[(Re\cdot x)^{1/2}\tan\theta]\}}\right\} \quad (4)$$

where $Q = \rho_\infty {u_\infty}^2/2$ and $S = \pi {r_w}^2$. Here positive $\bar{C}_f$ is in the positive z-direction (see Fig. 1).

For the local crossflow shear stress, we have

$$\tau = \int_0^{2\pi} (\mu w_y)_w r_w \cos\phi\,d\phi$$

After integrating along the body

$$(\bar{C}_f)_s = \frac{\bar{f}_s}{QS} = -\frac{2\sin\alpha\sin\theta}{S(Re)^{1/2}} \int_0^x (x)^{1/2}\,dx \int_0^{2\pi} \mu w_\eta\,d\phi \quad (5)$$

The effect of asymmetric viscous displacement on the Magnus force was first postulated by Martin[5] and Kelly.[19] This force can be approximately evaluated with slender body theory. Ward[23] has derived the following simple formula for the transverse force:

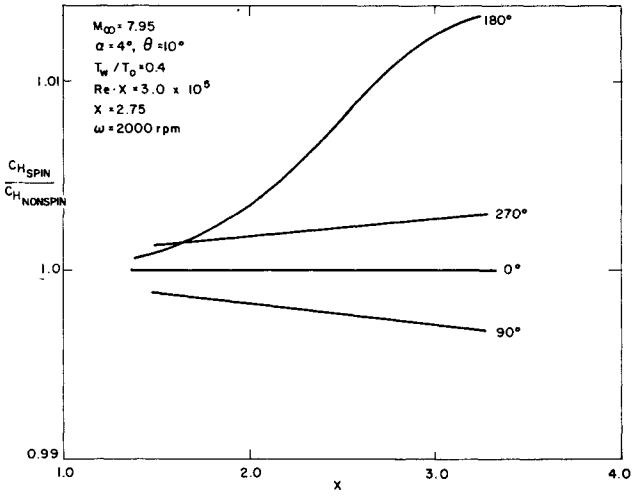

Fig. 7 Streamwise variation of normalized heat transfer.

$$(\bar{C}_f)_D = (\bar{f}_D/QS) = -2(d\bar{\mathscr{K}}/dx)$$

where

$$\bar{\mathscr{K}} = \bar{i}_l(x\sin\alpha + l_g) + z_g\bar{i}_z = \text{c.m. of the effective body}$$

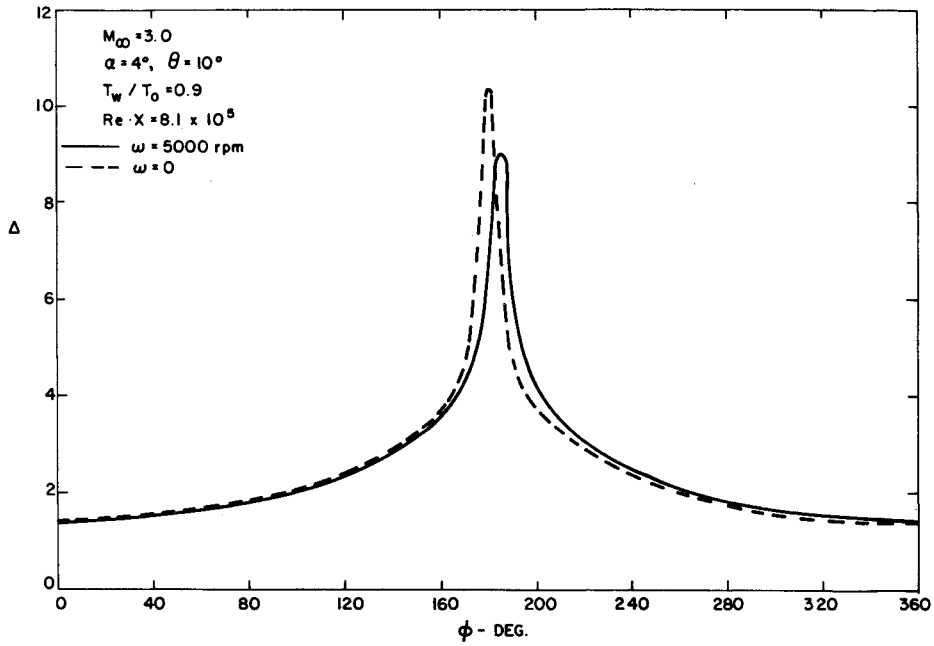

Fig 8 Displacement thickness distribution.

and

$$z_g \bar{i}_z + l_g \bar{i}_l = \frac{\int_0^{2\pi} \int_0^{(r_w+\Delta)} r^2\, dr\, d\phi(-\sin\phi \bar{i}_z + \cos\phi \bar{i}_l)}{\int_0^{2\pi} \int_0^{(\Delta+r_w)} r\, dr\, d\phi} \doteq \frac{1}{\pi}\int_0^{2\pi} \Delta(-\sin\phi \bar{i}_z + \cos\phi \bar{i}_l)\, d\phi \qquad (6)$$

Here Δ is the displacement thickness. As presented by Moore,[24] the following equation defines Δ:

$$\sin\theta \frac{\partial}{\partial x}[\rho_e u_e x(\Delta - \delta_x)] + \frac{\partial}{\partial \phi}[\rho_e w_e \sin\alpha(\Delta - \delta_\phi)] = 0$$

and

$$\delta_x = \int_0^\infty \left(1 - \frac{\rho u}{\rho_e u_e}\right) dy$$
$$\delta_\phi = \int_0^\infty \left(1 - \frac{\rho w}{\rho_e w_e}\right) dy \qquad (7)$$

Implicit in Eq. (6) is the assumption that $\Delta/r_w \ll 1$. The side force due to viscous displacement becomes

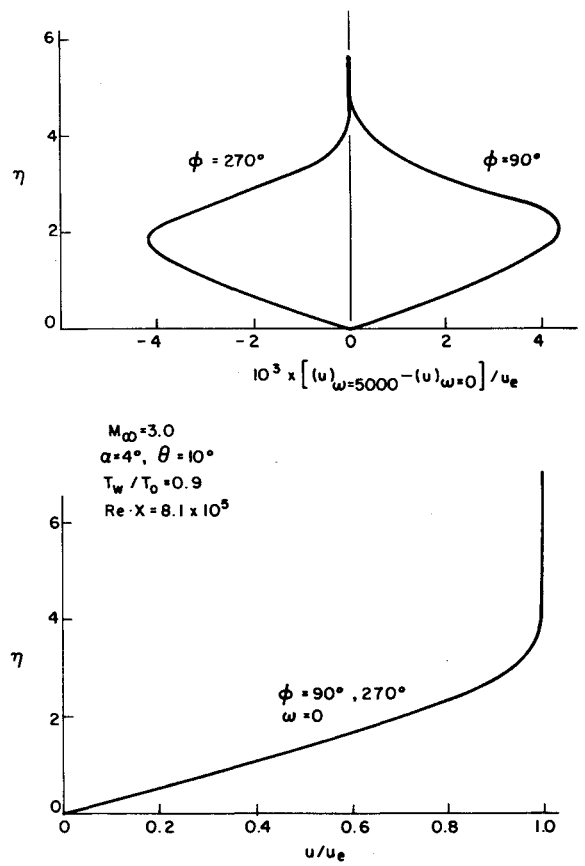

Fig. 9a Streamwise velocity profiles boundary layer.

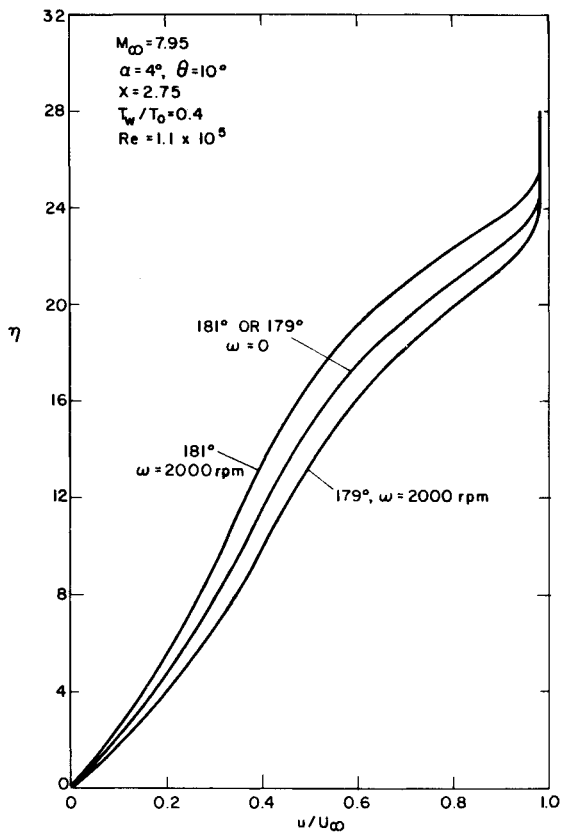

Fig. 9b Streamwise velocity profiles near leeward plane boundary layer.

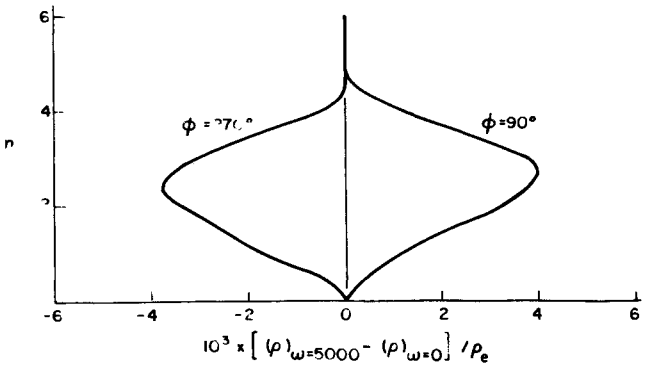

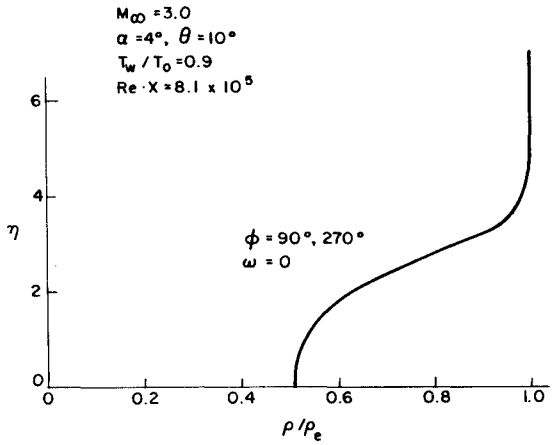

Fig. 9c Density distribution boundary layer.

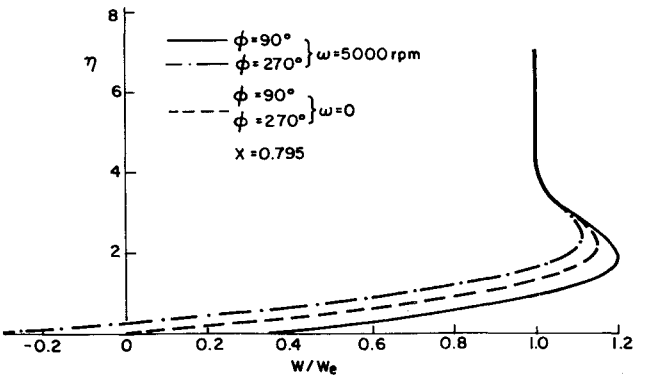

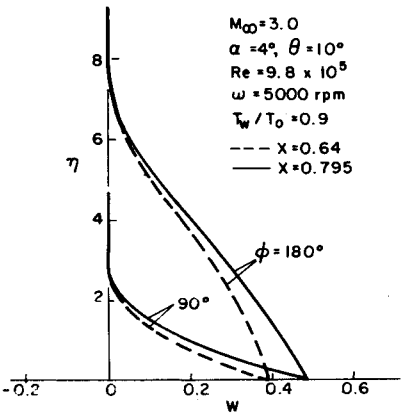

Fig. 9d Crossflow velocity profiles boundary layer.

$$(\bar{C}_f)_D = -\left[2\sin\alpha \bar{i}_l + \frac{1}{\pi}\int_0^{2\pi} \frac{d\Delta}{dx}(-\sin\phi \bar{i}_z + \cos\phi \bar{i}_l)\, d\phi\right] \quad (8)$$

where the $\bar{i}_l$ component represents the lift, and the $\bar{i}_z$ contribution leads to the Magnus force. Since Δ is the largest near the leeplane, the center of mass will move toward the leeward meridian (i.e., $l_g < 0$; see Fig. 1). Therefore, the viscous displacement effect will reduce the lift coefficient C_L obtained as $2\sin\alpha$ from slender body theory. This decrease in lift should not be confused with the increase in C_L associated with the shedding of vortices from the boundary layer into the potential flow. This latter phenomenon is a nonlinear effect which is not included in Ward's[23] theory. Finally, the transverse force in the z-direction becomes

$$(\bar{C}_f)_{Dm} = \frac{\bar{f}_{Dm}}{QS} = \frac{2}{(\pi Re)^{1/2}} \frac{d}{dx}\left(\int_0^{2\pi} \bar{x}^{1/2} \Delta \sin\phi\, d\phi\right) \quad (9)$$

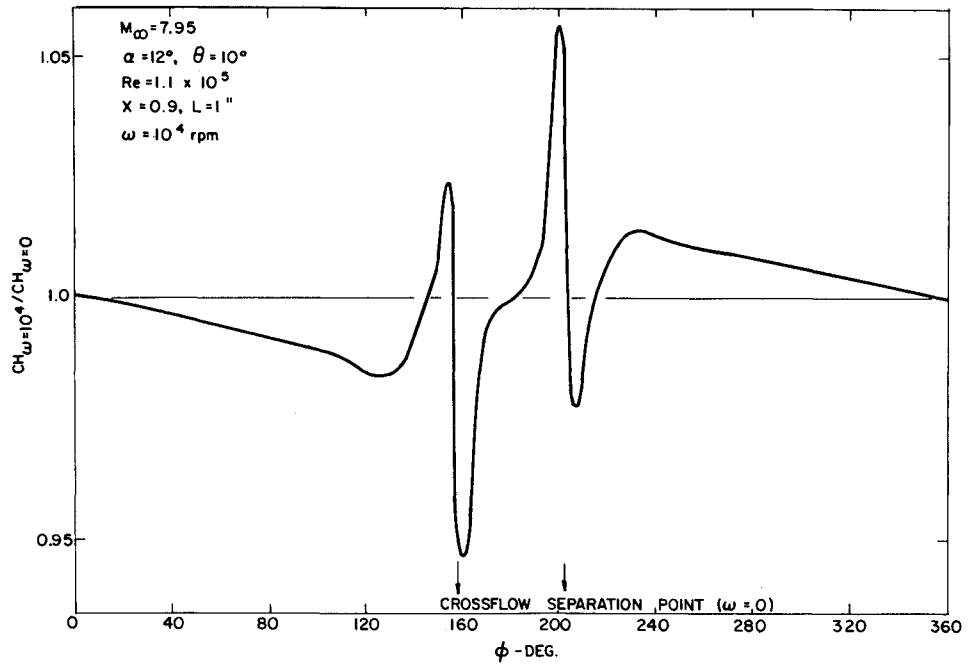

Fig. 10 Azimuthal distribution of heat transfer.

The total Magnus force is the sum of Eqs. (4, 5, and 9), i.e.,

$$\bar{f} = \bar{f}_{Dm} + \bar{f}_s + \bar{f}_{cf} \quad \text{and} \quad c_y = \bar{f}/QS \tag{10}$$

The Magnus coefficients are usually denoted by

$$C_{y\Omega} = C_y/\Omega$$
$$C_{y\Omega\alpha} = C_y/\Omega\alpha \tag{11}$$

The pitching moment can be shown to be

$$C_m = \frac{\int_0^x x\frac{d\bar{f}}{dx}dx}{QS(2r_w)} = \frac{x\bar{f}(x) - \int_0^x \bar{f}\,dx}{QS(2r_w)} \tag{12}$$

where the moment is referenced to the vertex of the cone. Finally, the Magnus moment coefficient is defined as

$$C_{m_{\Omega\alpha}} = C_m/\Omega\alpha$$

A simple trapezoidal rule is used to evaluate all the integrals.

The solutions for the Magnus coefficients on a spinning cone are depicted in Fig. 5. Also included is the data of Curry et al.[25] and the theoretical results of Sedney[4] and Vaughn and Reis.[9] The agreement between the present theoretical prediction and the experimental data is fair. It should be noted that the Vaughn and Reis theory includes the effects of viscous displacement and centrifugal force, whereas Sedney considered only the asymmetric boundary-layer displacement. The influence of wall cooling and the contributions of $C_{f_{cf}}$, C_{f_s}, $C_{f_{Dm}}$ are shown in Table 1. From these tabulated values it is found that the contributions due to

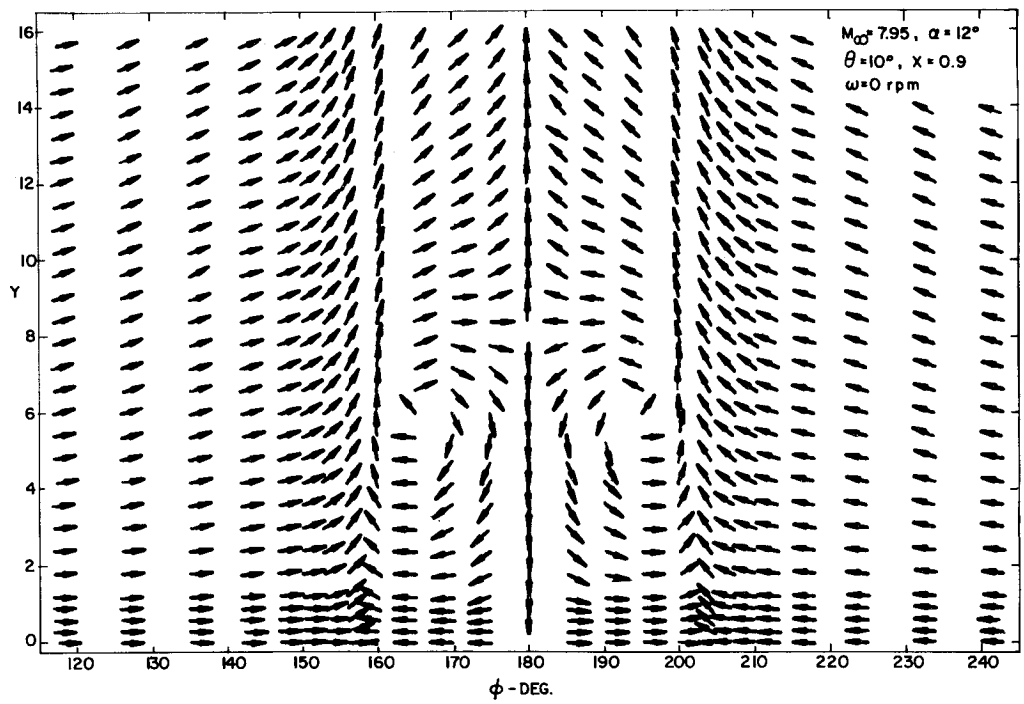

Fig. 11 Cross-plane (Y-ϕ) velocity vector projection.

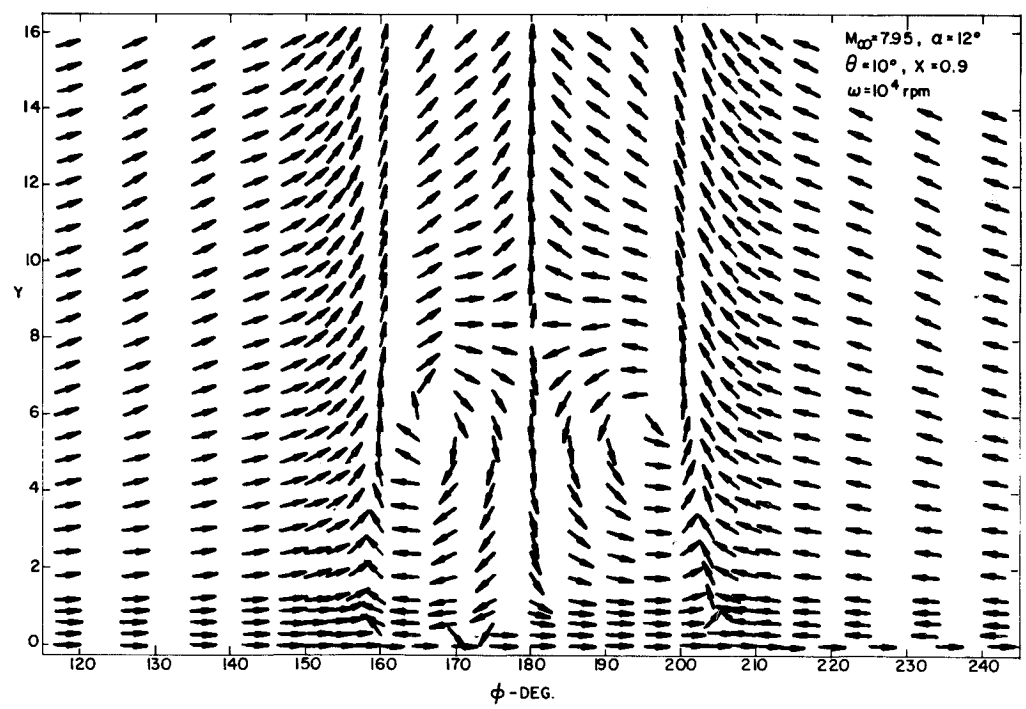

centrifugal force and crossflow drag are about the same order of magnitude but opposite in sign and will compensate each other. These effects are clearly not negligible; e.g., the meridional skin friction is about 20%–40% of that due to the displacement thickness. This is about the same as found from Sedney's results. For a cold wall, the Magnus forces and moments are an order of magnitude smaller than those found with a hot wall. Therefore, the Magnus phenomenon depends strongly on the surface temperature.

Figure 6 depicts the normalized heat transfer at $\alpha = 4°$ for $M_\infty = 3$ and 7.95. Only small variations due to spin are discerned except for a region near the leeward generator. The azimuthal gradients of temperature and boundary-layer thickness are comparatively large near $\phi = 180°$. The streamwise variation of heat transfer is presented in Fig. 7.

Shown in Fig. 8 is the displacement thickness distribution. Once again, the effects due to spin are small except near the leeward plane. Here Δ decreases at $180°^-$ and increases near $180°^+$. This distortion in Δ induces a Magnus force. For $\omega = 5000$ rpm and $x = 0.81$, the largest Δ is located at $\phi = 185°$ instead of $\phi = 180°$, and the peak values of Δ decrease due to spin.

The streamwise as well as crossflow velocity profiles and the density distribution are given in Fig. 9. The differences due to spin are found to occur in the third significant figure for u at $\phi = 90°$ and 270° (Fig. 9a); the profiles at $\phi = 179°$ and 181° have somewhat larger variations (Fig. 9b). The crossflow velocities in the η direction exhibit local maximum values for $\phi = 90°$ and 270°. This type of profile is somewhat different from the Vaughn and Reis "Blasius approximation," which is strictly valid for zero angle of attack.

The theories of Sedney and Vaughn and Reis predict a coupling between the angle of incidence and spin velocity; i.e., the term $\Omega\alpha \sin\phi$ appears in their analysis. This leads to a maximum asymmetry at $\phi = 90°$. In view of the numerical results for C_H and Δ presented here (Figs. 6 and 8), the simplified model is not substantiated. The maximum deviations are located very close to the leeward generator ($\phi = 180°$). The seemingly good agreement with the experimental Magnus coefficients, obtained by the approximate theories, is apparently due to the $\sin\phi$ weighting function appearing in the integrand of Eq. (9). This function is very small near the leeside, and hence the Magnus force is relatively insensitive to the boundary-layer behavior in this region.

Figure 10 illustrates the azimuthal distribution for the normalized C_H at an angle of attack $\alpha = 12°$ and $M_\infty = 7.95$. There are now two swirling vortices near the leeward plane as crossflow separation has occurred. The streamline projections at a fixed streamwise station are presented in Fig. 11. Here the streamline angle is denoted by

$$\Theta = \tan^{-1}(\bar{v}/\bar{w})$$

It can be seen from a comparison of the solutions for $\omega = 0$ and $\omega = 10^4$ rpm that the two vortices are displaced in the direction of spin. Considerably different flow patterns are discerned near and within the separation region.

By considering the conservation of mass for a streamtube near the surface, Lighthill[26] observed

$$\tfrac{1}{2}\rho q_y y^2 h = C = \text{Constant} \qquad (13)$$

where $q_y = [U_y^2 + W_y^2]^{1/2}$; h is the distance between two adjacent limiting streamlines and C is a constant equal to the massflow within the streamtube. The streamtube thickness y measured normal to the surface increases rapidly when either $q_y \to 0$, i.e., the friction vector vanishes, or when $h \to 0$. This latter case is associated with the formation of a free shear layer in the crossflow direction. Our numerical results exhibit behavior of the form indicated by Eq. (13). For example, the boundary-layer thickness along the crossflow separation line and the normal velocity V is comparatively large within this region (this can be seen from Fig. 11 at $\phi = 160°$ and 200°). Furthermore, the lateral diffusion terms, such as $U_{\phi\phi}$, must be retained if the free shear layer is to be adequately resolved.

VI. Summary

1) The Magnus forces and moments can be predicted by the numerical finite difference method presented herein. When the governing equations are correctly formulated and the numerical scheme is consistent with the physics, the calculations are stable and unique.

2) The asymmetric viscous displacement effect is the major contribution to the Magnus phenomena, although the contributions from the crossflow drag and the centrifugal force should not be neglected.

3) Surface temperature has a profound effect upon the magnitude of Magnus force.

4) The crossflow diffusion terms are important when a free shear layer forms. This occurs even at relatively small angle of incidence when crossflow separation and swirling vortex formation are not yet evident.

References

[1] Platou, A. S., "Magnus Characteristics of Finned and Nonfinned Projectiles," *AIAA Journal*, Vol. 3, No. 1, Jan. 1965, pp. 83–90.

[2] Fletcher, C. A. J., "The Magnus Characteristics of a Spinning Inclined Ogive Cylinder Body at Subcritical Reynolds Number in Incompressible Flow," WRE Rept. 423, June 1971, Weapons Research Establishment, Australia; see also *Journal of Aircraft*, Vol. 9, No. 12, Dec. 1972, pp. 826–834.

[3] Illingworth, C. R., "The Laminar Boundary Layer of a Rotating Body of Revolution," *Philosophy Magazine*, Ser. 7, Vol. 44, April 1953, pp. 389–403.

[4] Sedney, R., "Laminar Boundary Layer on a Spinning Cone at Small Angles of Attack in a Supersonic Flow," *Journal of Aerospace Sciences*, Vol. 24, June 1957, pp. 430–436.

[5] Martin, J. C., "On Magnus Effects Caused by the Boundary Layer Displacement Thickness on Bodies of Revolution at Small Angles of Attack," Rept. 870, June 1955, Army Ballistic Research Laboratories, Ballistic Research Laboratories, Aberdeen, Md.

[6] Clark, B. L., "Navier-Stokes Solutions for Laminar Incompressible Flow Over Yawed Spinning Bodies of Revolution," AIAA Paper 72-112, San Diego, Calif., 1972.

[7] Dwyer, H. A., "Hypersonic Boundary Layer Studies on a Spinning Sharp Cone at Angle of Attack," AIAA Paper 71-57, New York, 1971.

[8] Watkins, C. B., Jr., "Numerical Solutions of the Three-Dimensional Boundary Layer on a Spinning Sharp Body at Angle of Attack," Paper presented at the Symposium on Application of Computers to Fluid Dynamics Analysis and Design, 1973, Polytechnic Institute of Brooklyn, New York.

[9] Vaughn, H. R. and Reis, G. E., "A Magnus Theory," AIAA Paper 73-124, Washington, D.C., 1973.

[10] Lin, T. C. and Rubin, S. G., "Viscous Flow Over a Cone at Incidence. I-Hypersonic Tip Region," *International Journal of Computers and Fluids*, Vol. 1, No. 1, Jan. 1973, pp. 37–57.

[11] Rubin, S. G. and Lin, T. C., "A Numerical Method for Three-Dimensional Viscous Flow: Application to the Hypersonic Leading Edge," *Journal of Computational Physics*, Vol. 9, 1972, pp. 339–364.

[12] Lin, T. C. and Rubin, S. G., "Viscous Flow Over a Cone at Incidence. II-Supersonic Boundary Layer," PIBAL 72-27, Sept. 1972, Polytechnic Institute of Brooklyn, Brooklyn, N.Y.; see also *Journal of Fluid Mechanics*, Vol. 59, July 1973, pp. 593–620.

[13] Rubin, S. G., "A Predictor-Corrector Method for Three-Coordinate Viscous Flow," Paper presented at the 3rd International Symposium on Numerical Methods in Fluid Dynamics, July 1972, Paris, France.

[14] Helliwell, W. S. and Lubard, S. C., "Numerical Analysis of Separation on a Cone at High Angle of Attack," Paper presented at the Symposium on Application of Computers to Fluid Dynamics Analysis and Design, Jan. 1973, Polytechnic Institute of Brooklyn, Farmingdale, N.Y.

[15] Rubin, S. G., Lin, T. C., Pierucci, M., and Rudman, S., "Hypersonic Interaction Near Sharp Leading Edges," *AIAA Journal*, Vol. 7, No. 9, Sept. 1969, pp. 1744–1751.

[16] Novack, B. B. and Cheng, H. K., "Numerical Analysis and Modeling of Slip Flows at Very High Mach Numbers," *Lecture Notes in Physics*, Vol. 8, Springer-Verlag, Berlin, Sept. 1970, p. 503.

[17] Rubin, S. G. and Lin, T. C., "Rotational Non-Equilibrium Near a Hypersonic Leading Edge," Paper presented at the 7th International Rarefied Gas Dynamics Symposium, Pisa, Italy, 1970.

[18] Tracy, R. R., "Hypersonic Flow Over a Yawed Circular Cone,"

Hypersonic Research Project Memo 69, Aug. 1963, California Institute of Technology, Pasadena, Calif.

[19] Kelly, H. R., "An Analytical Method for Predicting the Magnus Force and Moments on Spinning Projectiles," TM-1634, 1954, U.S. Naval Ordnance Test Station, China Lake, Calif.

[20] Jones, D. L., "Tables of Inviscid Supersonic Flow about Circular Cones at Incidence $\gamma = 1.4$," AGARD 137, 1969.

[21] Mayne, A. W., "Analysis of Laminar Boundary Layers on Right Circular Cones at Angle of Attack, Including Streamline-Swallowing Effects," AEDC-TR-72-134, Oct. 1972, Arnold Engineering Development Center, Tullahoma, Tenn.

[22] Curry, W. H., Reed, J. F., and Ragsdale, W. C., "Magnus Data on the Standard 10° Cone Calibration Model," SC-DC 71-3821, 1971, Sandia Laboratories, Albuquerque, N. Mex.

[23] Ward, G. N., "Supersonic Flow Past Slender Pointed Bodies," *Quarterly Journal of Mechanics and Applied Mathematics*, Vol. 2, No. 1, March 1949, p. 75.

[24] Moore, F., "Displacement Effect of a Three-Dimensional Boundary Layer," TN 2722, 1952, NACA.

[25] Curry, W. H., Platou, A. S., and Reynold, W. C., "Magnus Characteristics of a 10° Cone at Supersonic Mach Numbers," Research Rept., Sandia Laboratories, Albuquerque, N. Mex. (to be published).

[26] Lighthill, M. J., *Laminar Boundary Layers*, edited by L. Rosenhead, Oxford Press, New York, 1963, pp. 1–113.

JULY 1974 AIAA JOURNAL VOL. 12, NO. 7

Prediction of the Critical Diameter of Composite Propellants

P. K. SALZMAN* AND T. C. DUNCAN†
General Dynamics, Pomona, Calif.

A theoretical model which predicts the critical diameter of composite propellants is presented. A previously published detonation model is corrected and refined by use of a new model which considers both single grain size AP and dual grain size AP configurations, for both porous and nonporous propellants. Both ignition due to shock heating of the AP and compression heating of gas-filled voids are considered. By comparison of results with experimental data for an AP-PBAN-Al propellant, an "intrinsic" porosity of 0.22% was established for nominally "nonporous" propellants. Using this value, a critical diameter of 3.0 ft is predicted for a nonaluminized AP propellant.

Nomenclature

a = length of a face centered cube (fcc)
a_o = nearest neighbor distance in a fcc
B = oxidizer burning rate
$\bar{B}$ = average burning rate
d = diameter
d_c = critical diameter
δ = diffusion/burning distance
δ_d = diffusion distance
D = detonation velocity
D_i = ideal detonation velocity
$\mathcal{D}$ = diffusion coefficient
ξ = reaction zone thickness
γ_g = Gruneisen's constant
n_p = total number of voids
N = number of "effective" voids (ignition sites)
P = propellant porosity
Q = heat of reaction
ρ = density
r_a = void radius
R_G = oxidizer grain radius
R_e = total burning distance
t = time
t_i = ignition time
t_o = oxidizer burning time
t_b = binder burning time
t_{ob} = oxidizer/binder burning time, nonconsecutive process
T = temperature
X = mass fraction

Subscripts
a = ambient conditions
Al = aluminum
B = binder
G = oxidizer (AP)
L = large grain
n = nonporous
S = small grain

Introduction

THE most important parameter in evaluating the detonability of a given substance is the critical diameter d_c. For composite propellants a theoretical method was developed[1] for predicting d_c based on an analysis of the events occurring in the reaction zone. It was shown that the d_c for nonporous propellant was quite high (~50 ft) but that it decreased rapidly with porosity P ($d_c \approx 1$ ft at $P \approx 5\%$). However, a subsequent experimental program[2] showed that d_c for (nonporous) composite propellants was actually much lower than predicted (~5 ft). The general objectives of the current study were to: 1) reconcile the differences in theory and experiment and develop an improved detonation model; and 2) apply the model to an AP-PVC/DOA propellant‡ to determine its d_c.

Detonation Model

The detonation model employed in this study is essentially that used in Ref. 1. The nozzle theory of Jones[3] is used to

Received November 27, 1972; presented as Paper 72-1117 at the AIAA/SAE 8th Joint Propulsion Specialist Conference, New Orleans, La., November 29–December 1, 1972; revision received October 29, 1973.

Index categories: Fuels and Propellants, Properties of; Shock Waves and Detonations; Combustion Stability, Ignition, and Detonation.

* Section Head, Aerothermodynamics Section. Member AIAA.
† Design Specialist.

‡ AP = Ammonium Perchlorate; PVC = Polyvinyl Chloride; and DOA = Di-Octyl Adipate.